Microelectronic Engineering 119 (2014) 100–104

Contents lists available at ScienceDirect

Microelectronic Engineering

journal homepage: www.elsevier.com/locate/mee

Solution-processed nanostructured zinc oxide cathode interfacial layers for efficient inverted organic photovoltaics

E. Polydorou [a], E. Makarona [a], A. Soultati [a], D.G. Georgiadou [a], T. Kyrasta [a], T. Speliotis [a], C. Tsamis [a], N. Papanikolaou [a], P. Argitis [a], I. Kostis [a,b], A. Kokkosis [a,b], D. Davazoglou [a], M. Vasilopoulou [a,*]

[a] Institute of Nanoscience and Nanotechnology (INN), National Center for Scientific Research "Demokritos", 153 10 Aghia Paraskevi Attikis, Athens, Greece
[b] Department of Electronics, Technological Educational Institute (TEI) of Piraeus, 12244 Aegaleo, Greece

ARTICLE INFO

Article history:
Received 17 October 2013
Received in revised form 4 March 2014
Accepted 11 March 2014
Available online 1 April 2014

Keywords:
Organic photovoltaics
Inverted structure
Zinc oxide
Nanostructured

ABSTRACT

Inverted organic photovoltaic (OPV) cells based on poly(3-hexylthiophene) (P3HT) as an electron donor and [6,6]-phenyl-C71-butyric acid methyl ester ($PC_{71}BM$) as an electron acceptor, were fabricated and characterized. To improve the photovoltaic performance, interface control using either dense or nanostructured ZnO films as cathode buffer layers for effective electron transport was demonstrated, while an under-stoichiometric transition metal oxide, such as MoO_x, was employed as the anode buffer layer for efficient hole extraction. Incorporation of a nanostructured ZnO interlayer enhanced electron–hole dissociation by enabling a larger interfacial contact with the active layer, that results in increased short-circuit current density (*Jsc*) and eventually contributing to higher power conversion efficiency (PCE).

1. Introduction

During the past decade organic photovoltaics (OPVs) have attracted great attention because of their light weight and potential low-cost manufacturability. In spite of their high power conversion efficiency achieved thus far, the commonly used conventional bulk-heterojunction (BHJ) architecture has limitations in terms of device stability due to the need for air-sensitive low work-function metal cathode, such as Al. Diffusion of oxygen into the active layer through pinholes and grain boundaries in the Al cathode may cause the degradation of the active layer, leading to device instability in air. One approach to solve this issue is using an inverted structure, where the charge separation and collection nature of the electrode is reversed [1]. In inverted structures, the highly acidic PEDOT:PSS – commonly used as the anode interfacial layer – can be avoided and replaced by a low-work function and stable-in-air metal oxide layer. In particular, titanium oxide (TiO_2) and zinc oxide (ZnO) appear to be promising cathode interfacial layers in organic optoelectronic devices due to their electronic structure and optical properties [1–6]. The addition of these metal oxide layers can enhance the performance of the device by creating an extra donor–acceptor interface or by acting as exciton blocking layers, which assist the charge collection and transport. In OPVs, apart from their role as electron extraction layers, they were initially used as optical spacers due to their adequate transparency [5–7]. In addition, by using TiO_2 and ZnO as interfacial layers between the active layer and the metal contact, the oxygen and moisture diffusion within the active layer that can cause damage to the device may be reduced resulting in enhanced environmental stability [8,9].

However, the metal oxide layers used in most studies are processed under high temperatures to increase their crystallinity for better charge mobility and transport. This disqualifies them to be used in organic solar cells. It is necessary that the devices are processed under low temperatures employing simpler methods so as to maintain flexibility and retain a thin form factor. In order to bypass the above-mentioned issues, inverted device architectures incorporating solution-processed n-type metal oxide layers deposited at low temperatures which can have high electron mobility to collect and transport electrons, can alternatively be used [10]. Compared to titanium oxide, ZnO exhibits high electron mobility and consequently it can be used as an ideal electron selective layer in inverted OPVs [11,12]. Until recently the ZnO electron selective layers in inverted OPVs were obtained by the atomic layer deposition (ALD) technique which is time consuming and increases the fabrication cost of the device [13,14]. Thus, solution-processed ZnO becomes more preferable because of its relatively easy fabrication in large quantities with low cost and compatibility with solution-processed OPVs [15]. Recently, ZnO nanostructures which

* Corresponding author. Tel.: +30 210 6503269; fax: +30 210 6511723.
E-mail address: mariva@imel.demokritos.gr (M. Vasilopoulou).

http://dx.doi.org/10.1016/j.mee.2014.03.006
0167-9317/

can be fabricated via various methods at relatively low temperature by a precursor solution under ambient conditions have attracted great attention [16–21]. Especially, the sol–gel method has been extensively investigated for the deposition of thin films from solutions [22,23]. However, sol–gel derived ZnO thin films form rough surfaces, which may cause large leakage current and extremely high contact resistance, deteriorating thus the inverted OPV devices. Therefore, it is critical to accurately control the deposition parameters of ZnO films in order to fabricate efficient OPV cells using these films as electron selective layers.

Herein, we report on an efficient inverted bulk-heterojunction solar cell based on poly(3-hexylthiophene):(6,6)-phenyl C_{71} butyric acid methyl ester (P3HT:PC_{71}BM) active layer with a highly uniform solution-processed nanostructured ZnO film used as electron selective layer and MoO_x as the hole selective layer. In particular, ZnO was deposited on the FTO anode on glass substrates using a low-cost and time-efficient all-wet technique that involves the formation of a seeding layer with the aid of a zero-gel solution, and a hydrothermal step for the formation of the ZnO nanostructured layer [24]. To highlight the impact of nanostructuring the ZnO layer a second device using a dense ZnO layer is also fabricated and characterized.

2. Experimental procedure

2.1. Zinc oxide nanostructured and dense films preparation

In more detail, the zero-gel consists of zinc acetate dehydrate dissolved in ethanol (analytical grade) and is applied on the substrate either by drop-casting or spin-coating depending on the application selected. Depending on the type of the substrate the number of applications may vary and can range from 3 to 10 times. The samples are then annealed in the presence of atmospheric air at temperatures over 250 °C for the Zn acetate particles spread on the substrate to calcinate into ZnO. The concentration of the zero-gel and the duration of the annealing are critical for the size of the resulting nanostructures [24]. For the ZnO nanoparticle/nanostructured-layer development, the process described in [25,26] was exploited, with the process parameters carefully selected and tailored to fit the requirements of inverted OPV architectures. In brief, the samples were suspended in aqueous equimolar solutions of zinc nitrate hexahydrate [$Zn(NO_3)2{\cdot}6H_2O$] and hexamine (HMTA) at 87 °C, while the concentration of the nutrients and the duration of the hydrothermal growth were selected based on the targeted geometrical characteristics of the nanostructured layers. Zinc acetate dehydrate and Zinc nitrate hexahydrate were purchased from Sigma–Aldrich and HMTA from Panreac and all were used without further purification.

2.2. Device fabrication and characterization

OPV devices were fabricated on fluorinated tin oxide (FTO) coated glass substrates (2 × 2 cm) with a sheet resistance 20 Ω/square, which served as the anode electrode. Substrates were ultrasonically cleaned with a standard solvent regiment (15 min each in acetone and isopropanol). The ZnO layer, with a thickness of approximately 40 nm, was then deposited followed by an approximately 100 nm photoactive layer. The active layer was consisting of P3HT:PC_{71}BM blend (1:0.8 wt.% ratio) and was spin-cast on top of the zinc oxide film from a 10 mg/ml chloroform solution. After being spin-coated, the active layer was annealed at 120 °C for 10 min in air. Then, an under-stoichiometric 10 nm-thick molybdenum oxide (MoO_x) layer was deposited on top of the active layer, using the previously reported hot-wire deposition method [27,28], to serve as the hole collection layer. The devices were completed with a 150 m thick aluminium cathode, deposited in a dedicated chamber. All chemicals were purchased from Sigma–Aldrich and used with no further purification. Film thickness was estimated with ellipsometry. Absorption measurements were taken using a Perkin Elmer Lampda 40 UV/Vis spectrophotometer.

2.3. Solar cells characterization

Current density–voltage characteristics of the fabricated solar cells were measured with a Keithley 2400 source-measure unit. Cells were illuminated with a Xe lamp and an AM 1.5G filter to simulate solar light illumination conditions with an intensity of 100 mW/cm^2 (1 sun), as was recorded with a calibrated silicon photodiode.

3. Results and discussion

Depending on the all-wet ZnO deposition parameters, more cohesive films of fused nanostructures (hereafter referred to as "dense films") or layers with distinct nanostructuring via the growth of uniform nanocrystallites (hereafter referred to as "nanostructured films") were obtained, as it can be seen from scanning electron microscopy (SEM) images shown in Fig. 1. Optical transmission spectra of the FTO-glass substrate pristine or covered by sol–gel ZnO processed under different conditions are shown in Fig. 2. Both FTO/ZnO substrates show good optical transparency as the pristine FTO substrate of over 80% average transmittance with little deviation within the visible optical spectrum. This observation suggests that the deposition of the ZnO layers on FTO cathode does not significantly affect the subsequent light harvesting. Thereby, using these ZnO-modified FTO glass as

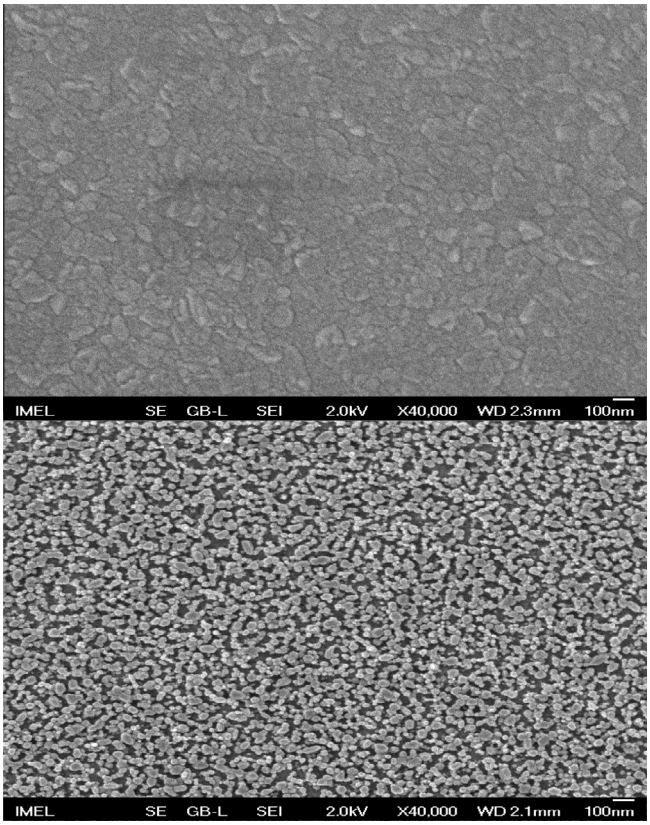

Fig. 1. Scanning electron microscopy (SEM) images of the ZnO layers used in this study. Top: dense layer; bottom: nanostructured layer. Both layers are about 40 nm thick.

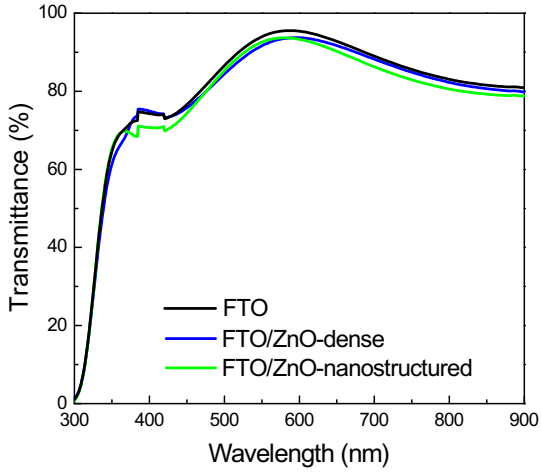

Fig. 2. Transmittance spectra of the two ZnO layers on FTO substrates with their SEM micrographs presented in Fig. 1. The spectrum of the FTO substrate is also shown.

transparent cathodes could allow the maximum photon flux to reach the BHJ layer for photocurrent generation. Additionally, the film transmittance of ZnO is slightly influenced by the process conditions because there is only a small shift towards small wavelength with the increasing films nanostructuring. The transmittance of FTO and both FTO/ZnO films is well above 90% in the range of 500–700 nm, which will beneficially affect the light harvesting of the BHJ layer, as well as the resulting device performance.

To get insights into these solution-processed ZnO films, their influence in device performance when incorporated as electron transporting layers was investigated. Both types of ZnO layers (dense and nanostructured) were embedded in reverse OPV devices to serve as electron collecting interlayers. The device structure is shown in Fig. 3a. This inverted structure employs the P3HT polymer as a donor material and the $PC_{71}BM$ as an acceptor material in the BHJ active layer. The n-type semiconducting ZnO films are sandwiched between the active layer and FTO as the cathode interface layer for electron transportation, and the MoO_x layer with hole injecting/extracting semiconductor characteristics is inserted between the Al anode and the BHJ layer as the anode interfacial layer for hole extraction. The relevant energy levels of all materials used in the inverted solar cells based on P3HT:$PC_{71}BM$, with the corresponding values taken from the literature [21,26], are shown in Fig. 3b.

Current density–voltage (*J–V*) characteristics of the inverted devices incorporating the ZnO films are shown in Fig. 4a. The photovoltaic parameters including photo conversion efficiency (PCE), open-circuit voltage (*Voc*), short-circuit current (*Jsc*), fill factor (*FF*), series resistance (*Rs*) and shunt resistance (*Rsh*) are summarized in Table 1. It can be clearly seen that the device performance of the inverted OPVs is significantly enhanced by using nanostructured ZnO cathode interfacial layers. The inverted device without ZnO, used as control, exhibited only a low PCE of 0.31% with a low *Voc* of 0.27 V, a *Jsc* of 4.54 mA cm^{-2} and an *FF* of 0.25. After incorporating the ZnO cathode interfacial layers, all of the photovoltaic parameters of inverted PSCs were remarkably improved. In particular, for the device embedding the dense ZnO layer the best PCE was improved to 1.41%, with a *Voc* of 0.51 V, a *Jsc* of 6.13 mA cm^{-2}, and an *FF* of 0.45 (Fig. 4a). In the case of the nanostructured ZnO incorporating device the above values were further

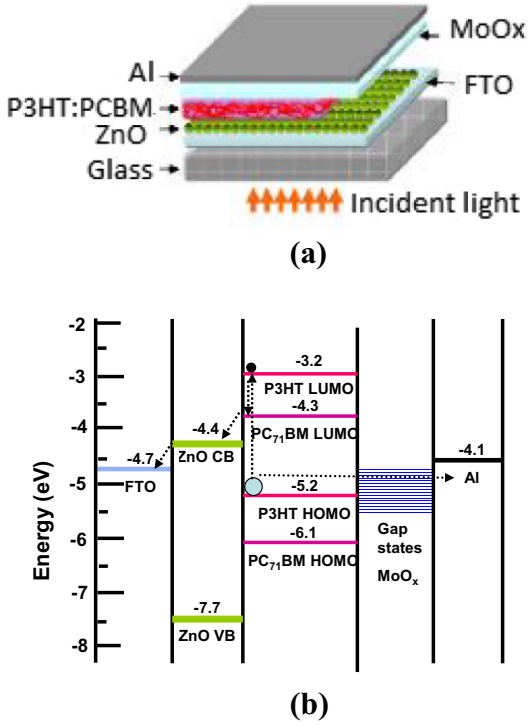

Fig. 3. (a) The OPV device with the reverse architecture and (b) the corresponding energy diagram (the relevant energy levels of the materials are obtained from the literature).

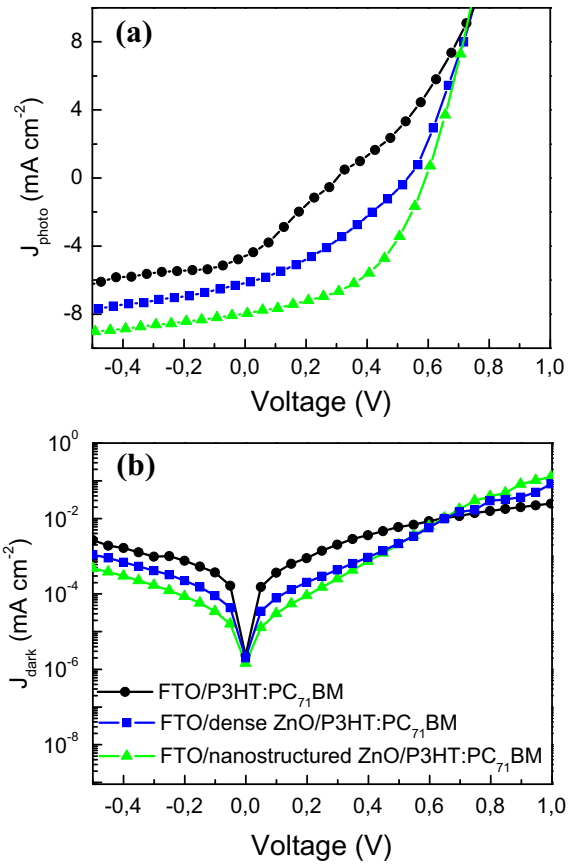

Fig. 4. (a) Current density versus voltage (*J–V*) characteristics measured under illumination with a 1.5 AM incident light and (b) dark *J–V* curves of P3HT:$PC_{71}BM$ based with or without ZnO electron extraction layers.

Table 1
Device characteristics of P3HT:PC71BM inverted OPV cells with the structure FTO/ZnO/P3HT:PC71BM/MoO_x/Al.

EEL	*Jsc* (mA/cm^2)	*Voc* (V)	*FF*	PCE (%)	*Rs* (Ω cm^2)	*Rsh* (Ω cm^2)
None	4.54	0.27	0.25	0.31	20	60
ZnO film	6.13	0.51	0.45	1.41	18	350
ZnO NPs	8.02	0.55	0.50	2.21	15	480

improved to a PCE of 2.21%, a *Voc* of 0.55 V, a *Jsc* of 8.02 mA cm^{-2} and an *FF* of 0.50.

The enhancement in devices performance after incorporating the ZnO layers can be attributed to the fine-matching energy levels and the formation of good Ohmic contacts between the BHJ layer and the ITO cathode when using the ZnO buffer layer. It has been known that the CBM and VBM of ZnO (with a wide band gap of ~3.3 eV) are about −4.4 eV and −7.7 eV, respectively [21]. As shown in Fig. 3b, the CBM of ZnO is very close to the energy level of the LUMO of $PC_{71}BM$ (~−4.3 eV), thus electrons can be efficiently extracted by the ZnO interlayers from the BHJ layer and transported to the ITO cathode through an energetically favourable pathway without significant loss in energy. Meanwhile, the use of ZnO buffer layers also prevents the direct contact between the active layer and the cathode, at the interface of which high densities of carrier traps or unfavorable interface dipoles may hinder the efficient charge collection. Using ZnO interlayers for good Ohmic contacts will maximize the *Voc*, because the reduction of the built-in potential causes an increment in dark current and carrier recombination. This result is also demonstrated by the corresponding *J–V* curves in the dark (Fig. 4b). By contrast, without the presence of the ZnO cathode interface layer, the BHJ layer directly contacts the cathode and good Ohmic contacts cannot be formed, since the work function of ITO (~−4.7 eV) is much deeper than the LUMO level of $PC_{71}BM$. It brings a large energy barrier formed at the cathode interface and produces a high contact resistance. Furthermore, the direct interfacing of the cathode and the BHJ layers does not allow efficient electron extraction, resulting in a significantly deteriorated device performance as evidenced by the extremely small *Rsh* of 60 Ω cm^2 and the large *Rs* of 20 Ω cm^2, compared to devices incorporating ZnO cathode buffer layers.

To further shed light into the mechanism responsible for the efficiency enhancement in devices embedding nanostructured ZnO, we also used a multiple scattering theory to calculate the optical properties of the multilayer structures [29,30]. The method is ideal for layered structures that include spherical scatterers. First, the electromagnetic problem is solved in each layer separately by obtaining the scattering S-matrix in a plane wave basis. Then, the S-matrix of the multilayer is calculated by appropriate combinations of the scattering matrices of each layer taking into account all multiple scattering events. For layers including periodic arrays of spheres, a spherical wave expansion is first used to describe the multiple scattering inside the layer, which a plane wave representation of the S-matrix is deduced from. Theoretical absorption spectra of the Glass/FTO/ZnO/P3HT:$PC_{71}BM$/MoO_x stacks are shown in Fig. 5a. The measured spectra of the same layered stacks are also shown in Fig. 5b. A small enhancement in the 350–550 nm wavelength region of the absorption spectrum of the stack in the case of the nanostructured ZnO is predicted by theory. The 350–550 nm is the wavelength region where the P3HT polymer donor absorbs strongly. Photons absorbed by the P3HT is very likely to convert into electron–hole pair and then into free carriers. The difference however, between the particles and the film is smaller in the theory compared to the experiment but the trend is correct. This is due to the fact that the P3HT:$PC_{71}BM$ that was assumed around the ZnO particles had $k = 0$. Absorption is due to the homogeneous P3HT:$PC_{71}BM$ layer (100 nm) just below the ZnO and was calculated with optical simulation using both films

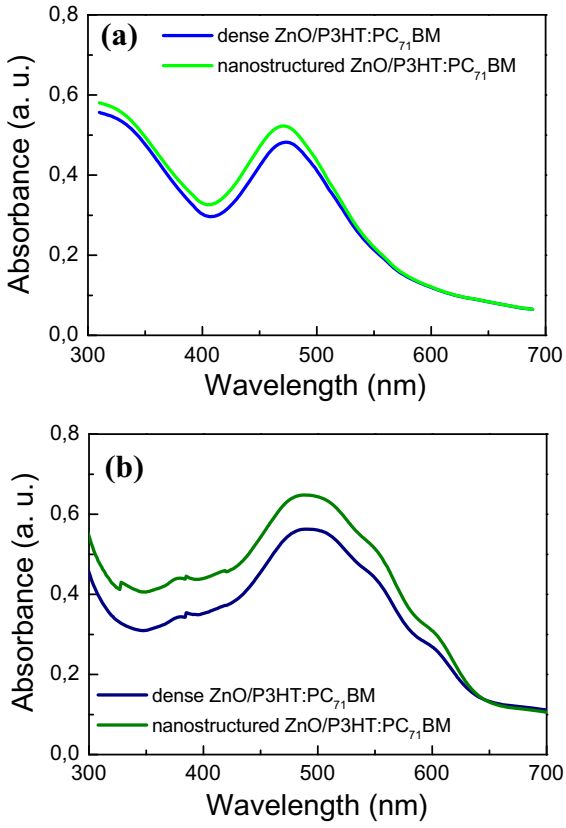

Fig. 5. (a) Calculated absorption spectra for normally incident light from the glass side on a multilayer: Glass ($n = 1.45$)/100 nm FTO ($n = 1.9$)/60 nm ZnO film ($n = 2$)/100 nm P3HT:PCBM/ 10 nm MoO_x ($n = 2.1$)/air (blue curve) and Glass ($n = 1.45$)/100 nm FTO ($n = 1.9$)/ZnO ($n = 2$) spherical particles (diameter = 60 nm on a square lattice, almost touching, embedded in a lossless P3HT:PCBM matrix)/100 nm P3HT:PCBM/10 nm MoO_x ($n = 2.1$)/air (green curve). The lossless matrix was modeled using the measured *n*, and setting $k = 0$. (b) The measured absorption spectra of the Glass/FTO/ZnO/P3HT:$PC_{71}BM$ multilayer stacks. (For interpretation of the references to colour in this figure legend, the reader is referred to the web version of this article.)

thicknesses and the experimental optical constants. The enhancement in light absorption in the case of the stack with the nanostructured ZnO layer is due to increased interfacial contact area which may also assist on more efficient exciton dissociation and, consequently, improvement in the device photocurrent.

4. Conclusions

We demonstrated the successful implementation of nanostructured ZnO as a promising solution for highly-efficient electron-extraction layers in inverted organic photovoltaic cells. In particular, we fabricated inverted BHJ solar cells based on a P3HT:$PC_{71}BM$ blend and transition metal oxide based cathode/anode interlayers. Interface control with either dense or nanostructured low-temperature solution-processed ZnO films as cathode interfacial layers and under-stoichiometric MoO_x as anode buffer layers provided effective charge extraction and transportation, leading to efficient inverted OPVs. The enhancement of current density and the overall

device performance improvement of the device incorporating the nanostructured ZnO layers is attributed to enhanced charge extraction/collection due to the efficient charge separation enabled by the large interfacial contact at the nanostructured ZnO/P3HT:$PC_{71}BM$ interface. Our results highlight the important role of metal oxide cathode/anode interlayers in determining the device photovoltaic parameters and also demonstrate that the interface engineering of metal oxide interlayers is a promising strategy to develop efficient and stable OPVs.

References

[1] K.K. Kyaw, X.W. Sun, C.Y. Jiang, G.Q. Lo, D.W. Zhao, D.L. Kwong, Appl. Phys. Lett. 93 (2008) 221107.
[2] S.H. Tsai, S.T. Ho, H.J. Jhuo, C.R. Ho, S.A. Chen, J.-H. He, Appl. Phys. Lett. 102 (25) (2013) 253111.
[3] C.-Y. Chen, J.R.D. Retamal, I.W. Wu, D.-H. Lien, M.-W. Chen, Y. Ding, Y.-L. Chueh, C.-I. Wu, J.-H. He, ACS Nano 6 (11) (2012) 9366–9372.
[4] A. Hayakawa, O. Yoshikawa, T. Fujieda, K. Uehara, S. Yoshikawa, Appl. Phys. Lett. 90 (16) (2007) 163517.
[5] L.-M. Chen, Z. Hong, G. Li, Y. Yang, Adv. Mater. 21 (14–15) (2009) 1434–1449.
[6] J.Y. Kim, S.H. Kim, H.H. Lee, K. Lee, W. Ma, X. Gong, A.J. Heeger, Adv. Mater. 18 (5) (2006) 572–576.
[7] J.Y. Kim, H. Lee, J. Park, D. Lee, H.-J. Song, J. Kwak, C. Lee, Jpn. J. Appl. Phys. 51 (2012) 10.
[8] J. Gilot, I. Barbu, M.M. Wienk, R.A.J. Janssen, Appl. Phys. Lett. 91 (11) (2007) 113520–113523.
[9] J. Liu, S. Shao, B. Meng, G. Fang, Z. Xie, L. Wang, X. Li, Appl. Phys. Lett. 100 (21) (2012) 213906.
[10] S.K. Hau, H.-L. Yip, N.S. Baek, J. Zou, K. O'Malley, A.K.Y. Jen, Appl. Phys. Lett. 92 (25) (2008) 253301–253303.
[11] Y. Sun, J.H. Seo, C.J. Takacs, J. Seifter, A.J. Heeger, Adv. Mater. 23 (14) (2011) 1679–1683.
[12] A.L. Roest, J.J. Kelly, D. Vanmaekelbergh, E.A. Meulenkamp, Phys. Rev. Lett. 89 (3) (2002) 036801.
[13] C. Zhang, H. You, Z. Lin, Y. Hao, Jpn. J. Appl. Phys. 50 (2011) 082302.
[14] J.-C. Wang, W.-T. Weng, M.-Y. Tsai, M.-K. Lee, S.-F. Horng, T.-P. Perng, C.-C. Kei, C.-C. Yu, H.-F. Meng, J. Mater. Chem. 20 (5) (2010) 862–866.
[15] M.S. White, D.C. Olson, S.E. Shaheen, N. Kopidakis, D.S. Ginley, Appl. Phys. Lett. 89 (14) (2006) 143517.
[16] M.A. Ibrahem, H.-Y. Wei, M.-H. Tsai, K.-C. Ho, J.-J. Shyue, C.W. Chu, Sol. Energy Mater. Sol. Cells 108 (2013) 156–163.
[17] Z. Liang, R. Gao, J.-L. Lan, O. Wiranwetchayan, Q. Zhang, C. Li, G. Cao, Sol. Energy Mater. Sol. Cells 117 (2013) 34–40.
[18] M. Wang, Y. Li, H. Huang, E.D. Peterson, W. Nie, W. Zhou, W. Zeng, W. Huang, G. Fang, N. Sun, X. Zhao, D.L. Carroll, Appl. Phys. Lett. 98 (10) (2011) 103305.
[19] Z. Hu, J. Zhang, Y. Liu, Z. Hao, X. Zhang, Y. Zhao, Sol. Energy Mater. Sol. Cells 95 (8) (2011) 2126–2130.
[20] P.S. Mbule, T.H. Kim, B.S. Kim, H.C. Swart, O.M. Ntwaeaborwa, Sol. Energy Mater. Sol. Cells 112 (2013) 6–12.
[21] M.J. Tan, S. Zhong, J. Li, Z. Chen, W. Chen, ACS Appl. Mater. Interfaces 5 (11) (2013) 4696–4701.
[22] M.N. Kamalasanan, S. Chandra, Thin Solid Films 288 (1–2) (1996) 112–115.
[23] A.K.K. Kyaw, X.W. Sun, C.Y. Jiang, G.Q. Lo, D.W. Zhao, D.L. Kwong, Appl. Phys. Lett. 93 (22) (2008) 221107.
[24] A. Kritharidou, Z. Georgoussi, C. Tsamis and E. Makarona, Proc. SPIE 8765, Art. No. 87650G–5.
[25] G. Niarchos, E. Makarona, C. Tsamis, Microsyst. Technol. 16 (2010) 669.
[26] Makarona, C. Fritz, G. Niarchos, Th. Speliotis, A. Arapoyanni and C. Tsamis, Proc. SPIE 8066, Art. No. 8066-53 (2011).
[27] M. Vasilopoulou, A.M. Douvas, D.G. Georgiadou, L.C. Palilis, S. Kennou, L. Sygellou, A. Soultati, I. Kostis, G. Papadimitropoulos, D. Davazoglou, J. Am. Chem. Soc. 134 (2012) 16178.
[28] M. Vasilopoulou, L.C. Palilis, D.G. Georgiadou, S. Kennou, I. Kostis, D. Davazoglou, P. Argitis, Appl. Phys. Lett. 100 (2012) 013311.
[29] N. Stefanou, V. Yannopapas, A. Modinos, Comp. Phys. Commun. 113 (1998) 49.
[30] N. Stefanou, V. Yannopapas, A. Modinos, Comp. Phys. Commun. 132 (2000) 189.